Laser Shock Forging — A novel in-situ method designed towards controlling residual stresses in Laser Metal Deposition

Yongkang Zhang
Shupeng Cai (caishupeng1991@sina.com)
Guangdong University of Technology https://orcid.org/0000-0002-9002-2478
Zhifan Yang
Ming Qiu
Zhengang Wang
Pingping Wu
Chi Xue
Xiaojian Huo

Research Article

Keywords: Hybrid in-situ method, Laser shock forging, Laser melting deposition, Inherent strain theory, Compressive residual stress

Posted Date: July 29th, 2022

DOI: https://doi.org/10.21203/rs.3.rs-1871824/v1

Version of Record: A version of this preprint was published at The International Journal of Advanced Manufacturing Technology on January 20th, 2023. See the published version at https://doi.org/10.1007/s00170-023-10874-8.

Abstract

This paper presents a novel hybrid in-situ additive manufacturing (AM) method —Laser Shock Forging (LSF), which combines laser shock peening (LSP) with laser melting deposition (LMD). Based on the classical Bar-frame model and inherent strain theory, the mechanisms of the effects of pretreatment and post-treatment on AM process has been firstly elaborated. Towards controlling tensile residual stress (TRS) in the as-built (AB) state of AM parts which has a detrimental effect on their fatigue life, we then developed LSF to introduce tensile inherent strains in LMD built parts in an in-situ manner, which will convert TRS to compressive residual stress (CRS). The laser beam used for shock peening can be adjusted to move synchronously with the laser beam used for metal deposition at a certain distance, ensuring the laser shock peening to act on the region where the material temperature cools down to the forging temperature range. Then experimental works have been conducted on 316L stainless steel, residual stress distributions of the AB, LSP and LSF treated specimens were compared, results show that LSF increases both the magnitude and depth of CRS compared with conventional LSP treatment, thus providing a promising application in enhancing fatigue life in AM process.

1. Introduction

In recent years, additive manufacturing (AM) [1–6] has attracted much attention due to its capabilities of fabricating complex geometry parts without dies, especially for those with internal features. It is realized by slicing the CAD model of a part into many thin layers, and then “print” each layer successively in a bottom-up manner, that’s why it’s also called “3D printing” [7–9]. The powder bed fusion (PBF) process is one of the most commonly used AM process for manufacturing complex metal parts, selective laser melting (SLM) [10–12] and electron beam melting (EBM) [13, 14] are classified to this category. At each step, a powder bed is deposited on a substrate and selectively melted by a scanning laser beam, after all the tracks in one layer are scanned, the substrate will be lowered down by a layer thickness to continue on the printing of next layer. On the other hand, directed energy deposition (DED) is more suitable for making repairs or adding features to an existing part, although it can also be used to build intact components. Laser melting deposition (LMD) [15, 16] and laser engineered net shaping (LENS) [17–19] are classified to this category. Compared with PBF, the size of the powder used by DED is larger and needs higher laser energy density, it has a faster building velocity but brings about lower surface quality which may need extra processing.

At the macroscopic scale, all these different metal AM processes that concerning about a moving high-energy heating source basically have similar physical processes which involves melting and solidification of metal [20]. Therefore, the large temperature gradient and high cooling rate occur due to intensive heat input and large local energy density will lead to accumulation of detrimental tensile residual stress (TRS) during the process [21–25]. This TRS distribution accounts for the geometrical inaccuracy, cracking, warpage, layer delamination and mechanical strength reduction of the AM built part, which leads to reduction of fatigue life and has to be eliminated as much as possible.

Many researches have been done to control and reduce residual stresses in additive manufacturing (AM) [26–32]. Preheating the substrate is a commonly used in-situ method [24]. It is found that adjusting laser scanning strategies have significant effect on the final residual stress distribution of AM built parts [14, 16, 30, 32, 33]. For post treatment, annealing is also a widely used method and can reduce 70% of residual stress in some cases. However, the methods mentioned above cannot fully convert TRS to compressive residual stress (CRS) which has been proved to capable of improving fatigue life of the built part. Moreover, in some cases where in-situ preheating or optimized scanning strategies cannot be successfully implemented, it will meet difficulty in building parts by AM.

In recent years, laser shock peening (LSP) as a novel surface treatment method has attracted much attention in its capability of enhancing fatigue life of AM built parts [34–37]. It can introduce CRS in the near surface layer of the material and deal with intricate parts with efficiency and accuracy. Compared with shot peening and ultrasonic shot peening [38–42], the CRS introduced by LSP has greater magnitude and deeper depth, thus has become a powerful post treatment to improve the fatigue life of the AM built parts.

However, it is still a post treatment and cannot introduce the bulk accumulation of high TRS during the AM building process. Kalentics et al. [43–47] proposed a novel hybrid AM process which they described as: “3D LSP” to successfully allow the 3D control of residual stress in SLM built parts. The method realized this by applying the LSP treatment every few SLM layers, which can obtain accumulated CRS in any critical zone in the bulk of the part. However, this method still needs careful re-alignment when the built parts comes to the rebuilding phase after LSP treatment, which is not an in-situ method and sacrifice manufacturing efficiency.

The inherent strain theory was first presented by Ueda et al. [48, 49] in late 70s and early 80s to predict the residual distortion and stress in metal welding process. Later in late 80s, Mura [50] described this inelastic strain as “eigenstrain”, he presented that eigenstrain is any kind of permanent strain due to inelastic process such as plastic deformation, crystallographic transformation, thermal expansion mismatch between different parts of assembly which causes incompatibility in the material, leading to the occurrence of residual stress distribution. In recent years, inherent strain theory has also been applied to analyze metal AM processes as they share similar characteristics with metal welding processes in which the materials will experience a cycle of heating and cooling and left with inherent strains [20, 28, 29, 31, 32, 51, 52]. In the AM built parts and heat-affected zone of welding pass, when the metal cools down to ambient temperature, there will be in-plane compressive inherent strains (usually inherent strain equals to plastic strain in this case if phase transformation is not considered) left, which are formed due to the constraint of the surrounding area during contraction. To counterbalance these compressive inherent strains, tensile residual elastic strains are formed, leading to TRS distribution in the as-built (AB) parts. As compressive inherent strains and its corresponding TRS distribution in the manufactured parts are not favorable for fatigue life, all the pretreatment or post-treatment are aiming at optimizing compressive inherent strain distribution, or converting them into positive. Obviously, preheating or optimizing scanning strategies belong to the former while LSP or “3D LSP” treatment belong to the latter.

In this paper, based on the classical Bar-frame model and inherent strain theory, we will firstly elaborate on the mechanisms of the effects of pretreatment and post-treatment on the manufacturing process concerning a cycle of heating and cooling. Towards introducing tensile in-plane inherent strains into the parts during the AM process, we then developed a novel hybrid method called “Laser Shock Forging” (LSF) to introduce tensile inherent strains in LMD built parts in an in-situ manner, the method has been patented by the Laboratory of Sino-US joint Laser Shot Peening at the Guangdong University of Technology (GDUT) [53]. By careful calibration of robotic arms, the laser beam used for shock peening can be adjusted to move synchronously with the laser beam used for metal deposition at a certain distance. The advantage of this method over LSP or “3D LSP” is that by adjusting distance between the two beams of laser, the laser shock peening can act on the region where the material temperature cools down to the forging temperature range, like a hammer forging on the metal just deposited by the scanning laser beam. In the forging temperature range, the material is easy to yield and larger tensile plastic strain can be induced. Then experimental works have been conducted on an austenitic 316L stainless steel, residual stress distributions of the AB, LSP and LSF treated specimens were compared, results have shown that LSF increases both the magnitude and depth of CRS compared with conventional LSP treatment, thus providing a promising application in enhancing fatigue life in AM process.

2. Basic Theories And Implementation Approach

2.1 Inherent strain theory and LSP treatment

The conventional LSP introduces positive plastic strain into the surface layer of the metal which induces compressive residual stress field due to elastic-plastic stress balance [54], as shown in Fig. 1. The introduced plastic strain in LSP is the source of inherent strain, which is any kind of permanent strain due to inelastic process such as plastic deformation, crystallographic transformation, thermal expansion mismatch between different parts of assembly which causes the incompatibility in the material, resulting in the existence of residual stress distribution. The inherent strain can be denoted as:

$$\varepsilon^* = \varepsilon_p + \varepsilon_{th}$$

1

where ε^* represents inherent strain, ε_p is plastic strain and ε_{th} is thermal strain, it is noted that in this paper, strain due to phase transformation has not been considered.

Warm laser shock peening (WLSP) [55] or laser shock peening without coatings (LSPwC) [56] are both designed to introduce larger tensile plastic strain (inherent strain) in the surface layer of the material, as higher temperature of the peening material or peening without ablative coatings will both cause the material easy to yield, thus leading to larger tensile inherent strain after LSP treatment.

2.2 Residual stress formation mechanism in LMD

The LMD process is a complicated manufacturing process in which the material experiences a cycle of heating and cooling, like the process of welding. As shown in Fig. 2, during the deposition, the material in front of the heat source (along the scanning direction) experiences thermal expansion due to the high energy input of laser beam, the expansion is constrained by the surrounding relatively less hot material, resulting in compressive stress in this region. After the heat source passes, the material cools down rapidly and begins to contract, then tensile residual stress field will be generated due to the constraint of the surrounding cold material. The similar kind of expansion and contraction cycle is also typical in the welding process, which is not favorable in the manufactured parts.

It is noted that tensile residual stress field is due to the compressive plastic strain formed in the heating and cooling cycles, which is the source of incompatibility in the material, in the inherent strain theory, if the material temperature cools down to ambient temperature, the inherent strain in the material is then denoted as:

$$\varepsilon^* = \varepsilon_p$$

2

Therefore, to reduce or eliminate the effect of tensile residual stress generated during the cycle of heating and cooling process, the key lies in reducing the compressive plastic strain formed in process.

2.3 Laser shock forging (LSF) designed for reducing tensile residual stress

For the research concerning using LSP to treat SLM or LMD built parts, the researchers aims to introduce tensile plastic strain in the built parts to counterbalance the compressive plastic strain generated by the cycle of heating and cooling. In order to make the LSP treatment more significant, Kalentics et al. [43–47] proposed the concept of “3D LSP”, in which laser shock peening is conducted after n-layers of SLM parts are built, the experimental results have shown that after “3D LSP” treatment a significant increase in the magnitude and depth of CRS has been observed when compared with as-built (AB) SLM parts and traditionally LSP parts.

As shown in Fig. 3, The primary difference between the proposed LSF approach in this paper and the “3D LSP” approach proposed by Kalentics et al. is that the laser beam used for shock peening moves synchronously with the laser beam used for metal deposition and they are kept at a certain distance, by careful calibration of robotic arms, the laser beam used for shock peening can be adjusted to the region where the material temperature cools down to the forging temperature range (usually 800℃-1250℃), thus the laser shock peening can acts like a hammer forging on the metal just deposited by the scanning laser beam, that’s why we present this novel process as “laser shock forging”.

2.4 Inherent mechanism for reduction of tensile residual stress

In order to explain the inherent mechanism for the reduction of tensile residual stress in LMD process, the classical Bar-frame model which has been used to illustrate the residual stress formation mechanism in the research of welding process is adopted [57]. As shown in Fig. 4, three rods of equal length are connected the rigid wall and the rigid body, the rigid wall is fixed while the rigid body can only move in one dimension. Assume that the materials of the rods are the same and they can only expand or contract in the direction of length, for simplification purpose, the rods are considered as perfectly elastic-plastic model, which means no strain hardening after yielding. Von Mises yield function and the associated flow rule is adopted, during the loading and unloading process, the Bauschinger effect is not considered.

The rod in the middle is uniformly heated to a temperature $T_{\max}$ ($T_{\max} < T_m$,T_m is the melting point) and then cools down to ambient temperature. There are maybe many possible stress-strain evolution cycles according to the magnitude of $T_{\max}$, we only take the most typical one in which $2T_Y < T_{\max} < T_m$, T_Y represents the temperature at which the uniaxial stress of the heated rod reaches the yield point and the stress state of the material turns from elastic to plastic.

As shown in Fig. 5, T represents current temperature and T_0 represents ambient temperature, the stress and strain evolves at different stages of heating and cooling, they can be characterized as follows:

I. Heating phase 1 ($T_0 < T < T_Y$,$|\sigma| < |\sigma_Y|$, O→A): as the temperature of the rod increases, the thermal strain can be calculated as:

$$\Delta\varepsilon_{t1} = \alpha\Delta T = \alpha(T - T_0)$$

3

where α represents the thermal expansion coefficient.

The rod has the tendency to expand in the length direction, however, its two ends are constrained by the rigid wall and rigid body, so uniaxial compressive strain and stress will be induced in the heated rod to remain stress equilibrium, the stress and strain will increase linearly before yielding as it is in elastic state.

II. Heating phase 2 ($T_Y \leqslant T < T_{\max}$,$|\sigma| = |\sigma_Y|$, A→B): as the material begins to yield, it enters into plastic state, because it is an perfectly elastic-plastic material, the yield stress will not increase any more, the material undergoes neutral loading while the total plastic strain will accumulate due to the presence of the plastic strain increment, this state is described in the following formulations:

$$\sigma_{\text{von}} = \sqrt{\frac{3}{2}\sigma' : \sigma'}$$

4

where σ_{von} is the von Mises stress, σ' is the deviatoric stress tensor.

The yield function is denoted as:

$$f = \sigma_{\mathrm{von}} - \sigma_Y$$

5

where σ_Y is the yield stress of the material.

When the yielding occurs, it follows that:

$$f(\sigma) = 0$$

6

By the associated flow rule the strain increment can be calculated as:

$$\mathrm{d}\,\varepsilon_p = \mathrm{d}\,\lambda \frac{\partial f}{\partial \sigma} = \mathrm{d}\,\lambda \cdot \sigma'$$

7

where $\mathrm{d}\,\lambda$ is a positive multiplier.

Then the total accumulated plastic strain can be calculated as:

$$\varepsilon_p = \int \mathrm{d}\,\varepsilon_p$$

8

As the temperature increases, the plastic strain keeps accumulating due to neutral loading, and attains at its maximum $\Delta\varepsilon_{p1} = \alpha(T_{\max} - T_Y)$ when $T = T_{\max}$. It has to be noted that in the heating phase, the accumulated plastic strain is compressive with a minus sign, the total accumulated plastic strain in the heating stage can be calculated as:

$$\Delta\varepsilon_{p1} = \alpha\Delta T = \alpha(T_{\max} - T_Y)$$

9

1. III. Cooling phase 1 ($T_{\max} - |T_Y| \leqslant T < T_{\max}$, B→Q): As the temperature reaches $T_{\max}$, it begins to cools down, the corresponding thermal strain gradually decreases, the rod enters from plastic state into elastic state to start elastic unloading, this stage proceeds until $\sigma = 0$, at that point, elastic strain vanishes, the compressive accumulated plastic strain and the thermal strain due to thermal expansion reach a balance to remain deformation compatibility.

2. IV. Cooling phase 2 ($T_{\max} - 2\left|T_Y\right| \leqslant T < T_{\max} - \left|T_Y\right|$, Q→C): As the temperature continues to decrease, the thermal strain also decreases, to remain deformation compatibility, the vanishing part of the thermal strain will then be compensated by the tensile elastic strain, thus the rod experiences a reverse elastic loading until yielding again, at that point $\sigma = \sigma_Y$.
3. V. Cooling phase 3 ($T_0 \leqslant T < T_{\max} - 2\left|T_Y\right|$, C→D): After reverse yielding, the material will experience neutral loading again, i.e. the yield stress remains at $\sigma = \sigma_Y$, and the accumulated plastic strain changes according to the plastic strain increment. As in the cooling phase the plastic strain increment is tensile with a plus sign, it is noted that the accumulated plastic strain will decrease in magnitude due to reverse loading, the total accumulated plastic strain in this stage can be calculated as:

$$\Delta\varepsilon_{p2} = \Delta\varepsilon_{t2} = \alpha\Delta T = \alpha(T_{\max} - 2\left|T_Y\right|)$$

10

Finally, when the rod cools down to ambient temperature, the plastic strain (inherent strain) left in the rod can be calculated as:

$$\varepsilon^* = \int_O^Q d\varepsilon_p + \int_Q^D d\varepsilon_p = \int_A^B d\varepsilon_p + \int_C^D d\varepsilon_p = \Delta\varepsilon_{p1} + \Delta\varepsilon_{p2} = -\alpha\left|T_Y\right|$$

11

It is shown that the inherent strain formed due to heating and cooling cycle is compressive, to remain deformation compatibility, the rod will subject to the same magnitude of tensile elastic strain, by Hooke's Law, this leads to tensile residual stress.

Taking a look at Eq. (11), the inherent strain consists of two components $\Delta\varepsilon_{p1}$ and $\Delta\varepsilon_{p2}$which are formed in the heating and cooling phase, respectively. $\Delta\varepsilon_{p1}$ is compressive while $\Delta\varepsilon_{p2}$ is tensile, as the magnitude of $\Delta\varepsilon_{p1}$ is larger than that of $\Delta\varepsilon_{p2}$, the final inherent strain is compressive. Therefore, the difference of their absolute value determines the final magnitude of residual stress. To reduce the residual stress due to the heating and cooling cycle, there are two routes designed for eliminating their difference: decrease the magnitude of $\Delta\varepsilon_{p1}$ or increase the magnitude of $\Delta\varepsilon_{p2}$.

For the first route, preheating is a favorable and commonly used method in welding and additive manufacturing [15, 24, 58]. It is explained that by preheating the material from ambient temperature to the maximum temperature, the temperature difference between T_Y and $T_{\max}$ will be narrowed, thus reducing the magnitude of $\Delta\varepsilon_{p1}$, while in the cooling phase the material will cool down to ambient temperature, the magnitude of $\Delta\varepsilon_{p2}$ remains unchanged, therefore, inherent strain and its induced residual stress will be reduced, as shown on the left side in Fig. 6.

For the second route, ultrasonic vibration [59–62] has been used in the welding process to reduce welding residual stress, the inherent reasons of which can be explained by Fig. 7. If in the elastic loading stage the

rod is imposed by an external excitation which causes the material to yield before cooling down to temperature $T_{\max} - 2\left|T_Y\right|$ (assume it is T_Y' in this case), and then cools down to ambient temperature T_0, the magnitude of $\Delta\varepsilon_{p2}$ will increase $\Delta\varepsilon_p'$ due to this excitation, while the magnitude of $\Delta\varepsilon_{p1}$ remains unchanged, therefore, inherent strain and its induced residual stress will be reduced. Actually, LSP treatment [34] or “3D LSP” treatment [44] of the SLM built parts does the same thing, they introduced tensile plastic strain into the surface layer of the SLM built parts to alleviate the compressive plastic strain induced by heating and cooling cycle, as shown on the right side in Fig. 6, this kind of treatment also increases the magnitude of $\Delta\varepsilon_{p2}$, but not in an in-situ manner.

Actually, the process of welding or AM is far more complicated than the proposed Bar-frame model, for instance, phase transformation [12] and work hardening [63] should both be considered in welding and AM. The case is more complicated for AM as the remelting of the previous layers and the surrounding material when scanning the next layer or pass should be considered [32], moreover, the constraint condition for the whole model is altering all the time due to its layer-by-layer building characteristic [27–29]. However, the Bar-frame model can shed some light on the routes designed for reducing residual stress induced in these thermal-related process.

Based on the above analysis, we have developed “laser shock forging” i.e. LSF method to come up with a way of controlling residual stress in LMD built parts. In this case, the laser beam used for shock peening acts as the “external excitation” which increases the magnitude of $\Delta\varepsilon_{p2}$ in an in-situ manner. By careful calibration of robotic arms, the laser beam used for shock peening can be adjusted to move synchronously with the laser beam used for metal deposition at a certain distance. The advantage of this method over LSP or “3D LSP” is that by adjusting distance between the two beams of laser, the laser shock peening can act on the region where the material temperature cools down to the forging temperature range (usually 800℃-1250℃), like a hammer forging on the metal just deposited by the scanning laser beam. In the forging temperature range, the material is easy to yield and larger tensile plastic strain can be induced. Besides, it is an in-situ and non-contact type of strengthening method, by comparison, LSP or “3D LSP” is not in-situ and needs careful realignment of the built parts, while ultrasonic vibration needs to contact the welding pass, which is not suitable for AM process.

3. Experimental Setups

3.1 Material and laser metal deposition

The material used in the experiment is the widely used 316L austenitic stainless steel, with an ultimate tensile strength (UTS) of 625 MPa. The powder used for LMD was provided by Guangdong Lei Ben Co. Ltd, China. Table 1 shows the chemical composition of the material and Fig. 8 shows its macro and micro morphology. Laser metal deposition was performed with a RC-LDM-2000-R (manufactured by Nanjing Zhongke Yihuan laser technology Co. Ltd, China) equipped with a fiber laser operated in continuous mode at a wave length 1064 nm and a spot size of 75 ~ 100 μm, as shown in Fig. 9. The specimen geometr y is a 30×20×10mm^3 cuboid and the base plate geometry is 140×140×8mm^3 sheet

with its material 1Cr13 mild steel. The chosen LMD processing parameters are shown in Table 2. A bi-directional scanning strategy parallel to the part edge was used to avoid creating large residual stress when changing the scanning direction between layers. Processing was performed under Ar atmosphere to avoid oxidation of the powder throughout the process.

Table 1
Chemical composition of 316L stainless steel, wt%

C	Si	Mn	P	S	Ni	Cr	Mo	Fe
0.02	0.55	1.55	< 0.03	< 0.03	10.0	16.5	2.08	Balance

Table 2
LMD processing parameters

Laser power	Spot diameter	Scanning speed	Hatching space	Layer thickness	Powder feeding rate
1500 W	3 mm	5 mm/s	1.5 mm	0.5 mm	40 g/min

3.2 Laser shock forging

Laser shock forging (LSF) experiments were done using the laser shock peening system “PROCUDO200” manufactured by LSPT Co. Ltd, the United States, as shown in Fig. 10. The laser source was a Nd: YLF with a pulse duration adjustable between 8 ~ 18ns and in this case is 18ns. The beam spatial energy distribution is “top-hat” and the pulse shape is near-Gaussian. The shape and size of laser spot is also adjustable and in this case is round with a diameter of 3 mm. The ratio of spot size and energy per pulse was adjusted carefully to keep a constant power density of 8 GW/cm^2. The pressure created at the surface of the part was estimated to 4.95 GPa using the following empirical equation:

$$P(GPa) = 1.75\sqrt{I_0}(GW/cm^2)$$

12

where I_0 is the power density of the laser beam.

Laser repetition frequency was 10 Hz, and the overlapping rate was 50% without a protective ablative layer. Detailed LSF processing parameters are shown in Table 3.

The key of the LSF process is to adjust the distance between the two laser beams to ensure the LSF acts on the deposited material whose temperature cools down to the forging temperature range. Due to the rapid solidification of the 316L stainless steel, the distance needs careful calibration. For the processing parameters used in this experiment, by many trial experiments, we finally determine that at a scanning speed of 5 mm/s of the laser beam for LM, the appropriate distance between the two laser beams is 0.40 mm.

Table 3
LSF processing parameters

Laser power	Laser energy	Spot diameter	Pulse duration	Repetition frequency	Overlapping rate
8 GW/cm^2	8 J	3 mm	18 ns	10 Hz	50%

3.3 Residual stress measurement using the X-ray diffraction method

Residual stress measurement was conducted using the X-ray diffraction method with a XL-640X X-ray stress tester manufactured by Shanghai Puchuang Technology Co. Ltd, China, as shown in Fig. 11. In-plane residual stress on the surface layer of the specimens was measured first, then the specimens are eroded layer by layer using an electro-polishing machine to measure the residual stress in the depth direction. A constant depth increment of 0.1 mm for electro-polishing erosion was applied and a maximum depth of 1 mm was measured for all the AB, LSP and LSF specimens.

4. Results And Discussion

To compare residual stress profiles of specimens due to different treatments, nine times of experiments were divided into three groups, number 1 ~ 3 are the specimens built by LMD; number 4–6 are firstly built by LMD and then treated by LSP; number 7–9 are the specimens built by LMD combined with LSF. To eliminate the effect of variable processing parameters, the laser parameters in LMD and LSP remain the same. After experiment, the specimens were cut from the base plate by electric discharge machining (EDM) and polished for residual stress measurement, each measurement point of the specimen are measured three times to obtain average data, then the data for the three specimens in each group will also be averaged to eliminate random errors.

4.1 As-built state

The as-built 316L LMD samples are shown in Fig. 12 and their averaged magnitude of residual stress are shown in Table 4. The high tensile value of 290 MPa at a depth of 0.1 mm accounts for 46% of the material UTS (630MPa). The typical stress distribution for samples manufactured by LMD remains tensile from the surface to the depth of > 1mm, as shown in Fig. 15.

4.2 LSP treated state

After LMD was done, the LMD samples were polished and covered with an ablative tape to be treated by LSP, Fig. 13 shows the specimens built by LMD before and after LSP. The measured residual stress value of LSP treated samples are also shown in Table 4, and the corresponding stress profiles are shown in Fig. 15.

From Table 4 it can be concluded that after LSP treatment, the initial TRS near the surface layer of the LMD parts have converted to CRS. The maximum magnitude of CRS is 320 MPa which occurs at the depth of 0.4 mm and CRS state remains at the depth of 0.65 mm.

4.3 LSF treated state

Figure 14 shows the specimens built by LMD combined with LSF, the comparisons of the measured residual stress values of the AB, LSP treated and LSF treated samples are shown in Table 4, and the corresponding stress profiles are shown in Fig. 15. It can be seen that LSF treated samples have gained greater magnitude of CRS and deeper depth of CRS state, compared with the LSP treated samples, an increase of 57% of the maximum magnitude of CRS has been presented.

During the LMD process, the laser shock peening acts on the region where the temperature lies in the forging temperature range (usually 800℃-1250℃ for 316L austenitic stainless steel), which acts like a hammer forging on the metal just deposited by the scanning laser beam, that's why we present this novel process as "laser shock forging". As the temperature is high enough for the material to yield, higher plastic deformation can be induced, measurement of residual stress profiles has shown that the melting and solidification of the successive layer has not led to full stress relaxation, thus CRS can accumulate through the whole bulk part during the building process. It has to be noted that optimal distance between the two beams of laser varies due to alternation of the material or laser scanning parameters, more experiments should be conducted to determine the relationship between optimal distance and the corresponding processing parameters, which is also our concentration on the future works.

Table 4
Comparisons of RS measurements/normalized by UTS, depth of maximum RS and depth of CRS.

Treatment	Max RS (MPa)/ percentage of the UTS(%)	Depth of max RS (mm)	Depth of CRS (mm)
AB	290/46	0.1	/
LSP	320/50.7	0.4	0.65
LSF	503/79.8	0.3	1

5. Conclusions And Future Works

In this paper, we have proposed a novel in-situ approach to controlling the residual stress state of LMD built parts by virtue of laser shock peening, which we called "Laser Shock Forging". The mechanism of the conversion from TRS to CRS has been explained by the classical Bar-frame model and inherent strain theory. The laser beam used for shock peening can be seen as the "external excitation" which increases the magnitude of compressive strain in an in-situ manner during the cooling phase. By careful calibration of robotic arms, the laser beam used for shock peening can be adjusted to move synchronously with the laser beam used for metal deposition at a certain distance.

The advantage of this method over LSP or “3D LSP” is that by adjusting the distance between the two laser beams, laser shock peening can act on the region where the material temperature cools down to the forging temperature range (usually 800℃-1250℃), like a hammer forging on the metal just deposited by the scanning laser beam. In the forging temperature range, the material is easy to yield and larger tensile plastic strain can be induced. Besides, it is an in-situ and non-contact type of strengthening method, by comparison, LSP or “3D LSP” is not in-situ and needs careful realignment of the built parts, while ultrasonic vibration needs to contact the welding pass, which is not suitable for AM process.

Experimental works have been conducted on an austenitic 316L stainless steel, in which a highly TRS state of the AB specimens can be converted into a CRS state. Residual stress distributions of the AB, LSP and LSF treated specimens were investigated, results have shown that LSF increases both the magnitude and depth of CRS compared with conventional LSP treatment, with an increase of 57% maximum magnitude and 54% depth. The means the melting and solidification of the successive layer has not led to full stress relaxation, CRS can therefore accumulate layer by layer.

As mentioned in the introduction, LMD is often used to make repairs in the manufactured components to enhance their fatigue life, by combing LSF with LMD we have achieved better performance in repairing cracks in the industry of aerospace and shipbuilding. Preliminary experimental results have shown that during LSF treatment the microstructure of the material will also change compared with AB and LSP state, future work will concentrate on the microstructure evolution and assessment of fatigue life of LSF treated specimens. The effects of the processing parameters including laser scanning speed, powder density, overlapping rate and laser spot size on the optimal distance between the two laser beams will also be investigated.

Declarations

Author contributions

Yongkang Zhang: Conceptualization; Participation in the whole work; Funding acquisition; Supervision; **Shupeng Cai:** Participation in the whole work, Writing of the article; data analysis and figure drawing; revision of the manuscript; **Zhifan Yang:** Data curation; **Ming Qiu**: Development of equipment; **Zhengang Wang**: Development of equipment; Pingping Wu: Development of equipment; **Chi Xue**: Development of equipment; **Xiaojian Huo**: Development of equipment. All authors read and approved the final manuscript.

Funding

The presented investigations have been supported by the National Natural Science Foundation of China (No. 51775117). Research and demonstration of the key technologies for the next-generation deep-water offshore ultra-large wind turbine installation platforms (No. 502200029). All the supports above are greatly acknowledged.

Availability of data and material Not applicable.

Code availability Not applicable.

Ethics approval Not applicable.

Conflict of interest

The authors declare that they have no conflict of interests.

References

1. Dai K, Shaw L (2004) Thermal and mechanical finite element modeling of laser forming from metal and ceramic powders. Acta Mater 52:69–80
2. Dai K, Shaw L (2005) Finite element analysis of the effect of volume shrinkage during laser densification. Acta Mater 53:4743–4754
3. Mercelis P, Kruth JP (2006) Residual stresses in selective laser sintering and selective laser melting. Rapid Prototyp J 12(5):254–265
4. Roberts IA, Wang CJ, Esterlein R, Stanford M, Mynors DJ (2009) A three-dimensional finite element analysis of the temperature field during laser melting of metal powders in additive layer manufacturing. Int J Mach Tool Manu 49:916–923
5. Verhaeghe F, Craeghs T, Heulens J, Pandelaers L (2009) A pragmatic model for selective laser melting with evaporation. Acta Mater 57:6006–6012
6. Yadroitsev I, Gusarov A, Yadroitsava I, Smurov I (2010) Single track formation in selective laser melting of metal powders. J Mater Process Tech 210:1624–1631
7. Yin J, Zhu HH, Ke LD, Lei WJ, Dai C, Zuo DL (2012) Simulation of temperature distribution in single metallic powder layer for laser micro-sintering. Comp Mater Sci 53:333–339
8. Hussein A, Hao L, Yan CZ, Everson R (2013) Finite element simulation of the temperature and stress fields in single layers built without-support in selective laser melting. Mater Des 52:638–647
9. Khairallah SA, Anderson A (2014) Mesoscopic simulation model of selective laser melting of stainless steel powder. J Mater Process Tech 214:2627–2636
10. Loh LE, Chua CK, Yeong WY, Song J, Mapar M, Sing SL, Liu ZH, Zhang DQ (2015) Numerical investigation and an effective modelling on the Selective Laser Melting (SLM) process with aluminium alloy 6061. Int J Heat Mass Transfer 80:288–300
11. Cheng B, Shrestha S, Chou K (2016) Stress and deformation evaluations of scanning strategy effect in selective laser melting. Addit Manuf 12:240–251

12. Huang Y, Yang LJ, Du XZ, Yang YP (2016) Finite element analysis of thermal behavior of metal powder during selective laser melting. Int J Therm Sci 104:146–157
13. Prabhakar P, Sames WJ, Dehoff R, Babu BB (2015) Computational modeling of residual stress formation during the electron beam melting process for Inconel 718. Addit Manuf 7:83–91
14. Robinson J, Ashton I, Fox P, Jones E, Sutcliffe C (2018) Determination of the effect of scan strategy on residual stress in laser powder bed fusion additive manufacturing. Addit Manuf 23:13–24
15. Yang QC, Zhang P, Cheng L, Min Z, Chyu M, To AC (2016) Finite element modeling and validation of thermomechanical behavior of Ti-6Al-4V in directed energy deposition additive manufacturing. Addit Manuf 12:169–177
16. Wang JS, Zhang JJ, Liu GT, Liang LJ, Yang G, Huang AG, Pang SY (2022) Effects of scanning strategies on residual stress and deformation by high-power direct energy deposition Island size and laser jump strategy between islands. J Manuf Process 75:23–40
17. Palcic I, Balazic M, Milfelner M, Buchmeister B (2009) Potential of laser engineered net shaping (LENS). Technol Mater Manuf Process 24(7–8):750–753
18. Mudge RR, Wald NR (2007) Laser engineered net shaping advances additive manufacturing and repair. Weld J 86(1):44–48
19. Li LJ (2006) Repair of directionally solidified superalloy GTD-111 by laser-engineered net shaping. J Mater Sci 41(23):7886–7893
20. Liang X, Cheng L, Chen Q, Yang QC, To AC (2018) A modified method for estimating inherent strains from detailed process simulation for fast residual distortion prediction of single-walled structures fabricated by directed energy deposition. Addit Manuf 23:471–486
21. Vastola G, Zhang G, Pei QX, Zhang YW (2016) Controlling of residual stress in additive manufacturing of Ti6Al4V by finite element modeling. Addit Manuf 12:231–239
22. Afazov S, Denmark WAD, Toralles BL, Holloway A, Yaghi A (2017) Distortion prediction and compensation in selective laser melting. Addit Manuf 17:15–22
23. An K, Yuan L, Dial L, Spinelli I, Alexandru DS, Gao Y (2017) Neutron residual stress measurement and numerical modeling in a curved thin-walled structure by laser powder bed fusion additive manufacturing. Mater Des 135:122–132
24. Li YL, Zhou K, Tan PF, Tor SB, Chua CK, Leong KF (2018) Modeling temperature and residual stress fields in selective laser melting. Int J Mech Sci 136:24–35
25. Bartlett JL, Li XD (2019) An overview of residual stresses in metal powder bed fusion. Addit Manuf 27:131–149
26. Bugatti M, Semeraro Q (2018) Limitations of the inherent strain method in simulating powder bed fusion processes. Addit Manuf 23:329–346
27. Chen Q, Liu JK, Liang X, To AC (2020) A level-set based continuous scanning path optimization method for reducing residual stress and deformation in metal additive manufacturing. Comput Method Appl M 360:112719

28. Liang X, Dong W, Hinnebusch S, Chen Q, Tran HT, Lemon J, Cheng L, Zhou ZK, Hayduke D, To AC (2020) Inherent strain homogenization for fast residual deformation simulation of thin-walled lattice support structures built by laser powder bed fusion additive manufacturing. Addit Manuf 32:101091
29. Takezawa A, To AC, Chen Q, Liang X, Dugast F, Zhang XP, Kitamura M (2020) Sensitivity analysis and lattice density optimization for sequential inherent strain method used in additive manufacturing process. Comput Method Appl M 370:113231
30. Chen Q, Taylor H, Takezawa A, Liang X, Jimenez X, Wicker R, To AC (2021) Island scanning pattern optimization for residual deformation mitigation in laser powder bed fusion via sequential inherent strain method and sensitivity analysis. Addit Manuf 46(S1):102116
31. Dong W, Liang X, Chen Q, Hinnebusch S, Zhou ZK, To AC (2021) A new procedure for implementing the modified inherent strain method with improved accuracy in predicting both residual stress and deformation for laser powder bed fusion. Addit Manuf 47:102345
32. Liang X, Dong W, Chen Q, To AC (2021) On incorporating scanning strategy effects into the modified inherent strain modeling framework for laser powder bed fusion. Addit Manuf 37:101648
33. Parry I, Ashcroft IA, Wildman RD (2016) Understanding the effect of laser scan strategy on residual stress in selective laser melting through thermo-mechanical simulation. Addit Manuf 12:1–15
34. Lv JM, Luo KY, Lu HF, Wang Z, Liu JJ, Lu JZ (2022) Achieving high strength and ductility in selective laser melting Ti-6Al-4V alloy by laser shock peening. J Alloy Compd 899:163335
35. Jin XY, Lan L, Gao S, He B, Rong YH (2020) Effects of laser shock peening on microstructure and fatigue behavior of Ti-6Al-4V alloy fabricated via electron beam melting. Mater Sci Eng A 780:139199
36. Lan L, Jin XY, Gao S, He B, Rong YH (2020) Microstructural evolution and stress state related to mechanical properties of electron beam melted Ti-6Al-4V alloy modified by laser shock peening. J Mater Sci Technol 50:153–161
37. Tong ZP, Pan XY, Zhou WF, Yang Y, Ye YX, Qian DS, Ren XD (2021) Achieving excellent wear and corrosion properties in laser additive manufactured CrMnFeCoNi high-entropy alloy by laser shock peening. Surf Coat Technol 422:127504
38. Fabbro R, Fournier J, Ballard P, Devaux D, Virmont J (1990) Physical study of laser-produced plasma in confined geometry. J Appl Phys 68(2):775–784
39. Berthe L, Fabbro R, Peyre P, Tollier L, Bartnicki E (1997) Laser induced shock waves as surface treatment for 7075-T7351 aluminium alloy. J Appl Phys 828(6):2826–2832
40. Ruschau JJ, John R, Thompson SR, Nicholas T (1999) Fatigue crack nucleation and growth rate behavior of laser shock peened titanium. Int J Fatigue 21:S199–S209
41. Hatamleh O, Lyons J, Forman R (2007) Laser and shot peening effects on fatigue crack growth in friction stir welded 7075-t7351 aluminum alloy joints. Int J Fatigue 29(3):421–434
42. Dorman M, Toparli MB, Smyth N, Cini A, Fitzpatrick ME, Irving PE (2012) Effect of laser shock peening on residual stress and fatigue life of clad 2024 aluminium sheet containing scribe defects. Mater Sci Eng A 548:142–151

43. Kalentics N, Boillat E, Peyre P, Ciric-Kostic S, Bogojevic N, Logé RE (2017) Tailoring residual stress profile of Selective Laser Melted parts by Laser Shock Peening. Addit Manuf 16:90–97
44. Kalentics N, Boillat E, Peyre P, Gorny C, Kenel C, Leinenbach C, Jhabvala J, Logé RE (2017) 3D Laser Shock Peening – A new method for the 3D control of residual stresses in Selective Laser Melting. Mater Des 130:350–356
45. Kalentics N, Burn A, Cloots M, Logé RE (2019) 3D laser shock peening as a way to improve geometrical accuracy in selective laser melting. Int J Adv Manuf Tech 101(5–8):1247–1254
46. Kalentics N, Sohrabi N, Tabasi HG, Griffiths S, Jhabvala J, Leinenbach C, Burn A, Logé RE (2019) Healing cracks in selective laser melting by 3D laser shock peening. Addit Manuf 30:100881
47. Kalentics N, Seijas M, Griffiths S, Leinenbach C, Logé RE (2020) 3D laser shock peening – A new method for improving fatigue properties of selective laser melted parts. Addit Manuf 33:101112
48. Ueda Y, Fukuda K, Nakacho K, Endo S (1975) A new measuring method of residual stresses with the aid of finite element method and reliability of estimated values. J Soc Nav Archit Jpn 138:499–507
49. Ueda Y, Kim YC, Yuan MG (1989) A predicting method of welding residual stress using source of residual stress (report I): characteristics of inherent strain (source of residual stress)(mechanics, strength & structural design). Trans JWRI 18(1):135–141
50. Mura T (1987) Micromechanics of defects in solids. Martinus Nijhoff, Dordrecht
51. Chen Q, Liang X, Hayduke D, Liu JK, Cheng L, Oskin J, Whitmore R, To AC (2019) An inherent strain based multiscale modeling framework for simulating part-scale residual deformation for direct metal laser sintering. Addit Manuf 28:406–418
52. Liang X, Chen Q, Cheng L, Hayduke D, To AC (2019) Modified inherent strain method for efficient prediction of residual deformation in direct metal laser sintered components. Comput Mech 64(6):1719–1733
53. Zhang YK, Yang QT, Yang ZF, Zhang Z, Yu QY (2020) "Method for rapidly forming a part using combination of arc deposition and laser shock forging and device implementing same". United States Patent Application US10682716B2
54. Cai SP, Zhang YK (2022) An iterative approach combined with multi-dimensional fitting of limited measured stress points to reconstruct residual stress field generated by laser shock peening. Surf Coat Technol 436:128237
55. Prabhakaran S, Kalainathan S (2016) Warm laser shock peening without coating induced phase transformations and pinning effect on fatigue life of low-alloy steel. Mater Des 107:98–107
56. Sano Y, Masaki K, Gushi T, Sano T (2012) Improvement in fatigue performance of friction stir welded A6061-T6 aluminum alloy by laser peening without coating. Mater Des 36:809–814
57. Goldak J, Akhlaghi M (2006) Computational welding mechanics. Springer Science & Business Media
58. Luo C, Qiu JH, Yan YG, Yang JH, Uher C, Tang XF (2018) Finite element analysis of temperature and stress fields during the selective laser melting process of thermoelectric SnTe. J Mater Process Tech 261:74–85

59. Elangovan S, Semeer S, Prakasan K (2009) Temperature and stress distribution in ultrasonic metal welding-An FEA-based study. J Mater Process Tech 209(3):1143–1150
60. Chen C, Fan CL, Lin SB, Cai XY, Yang CL, Zhou L (2019) Influence of pulsed ultrasound on short transfer behaviors in gas metal arc welding. J Mater Process Tech 267:376–383
61. Chen C, Fan CL, Cai XY, Lin SB, Yang CL, Zhuo YM (2020) Microstructure and mechanical properties of Q235 steel welded joint in pulsed and un-pulsed ultrasonic assisted gas tungsten arc welding. J Mater Process Tech 275:116335
62. Hu YY, Liu HJ, Fujii H (2019) Improving the mechanical properties of 2219-T6 aluminum alloy joints by ultrasonic vibrations during friction stir welding. J Mater Process Tech 271:75–84
63. Smith MC, Bouchard PJ, Turski M, Edwards L, Dennis RJ (2012) Accurate prediction of residual stress in stainless steel welds. Comp Mater Sci 54:312–328

Figures

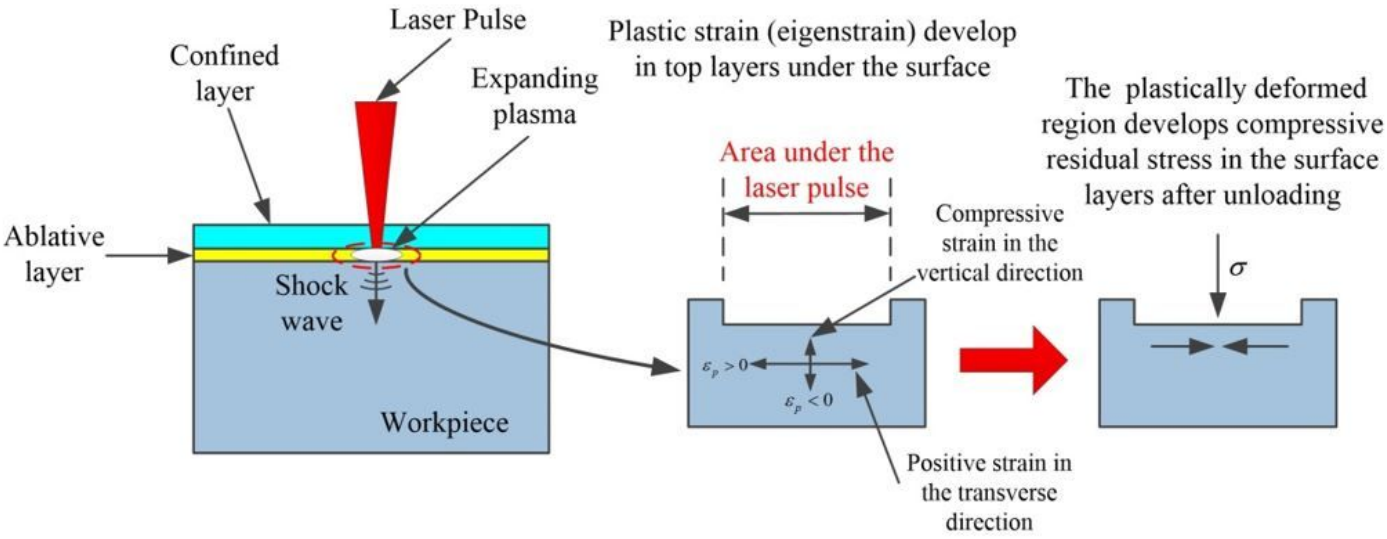

Figure 1

A schematic view of laser shock peening [53].

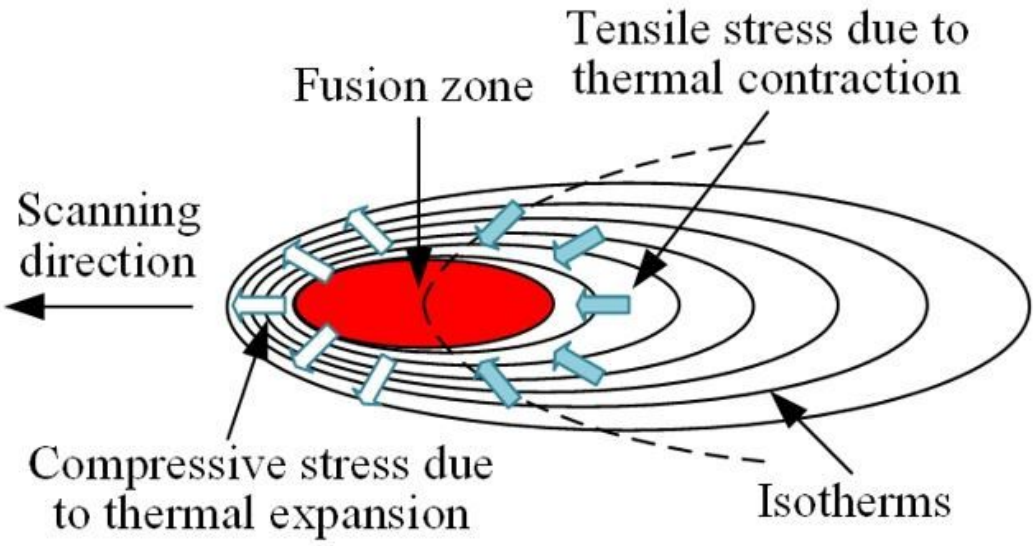

Figure 2

A schematic view of the thermal expansion and contraction around the heat source.

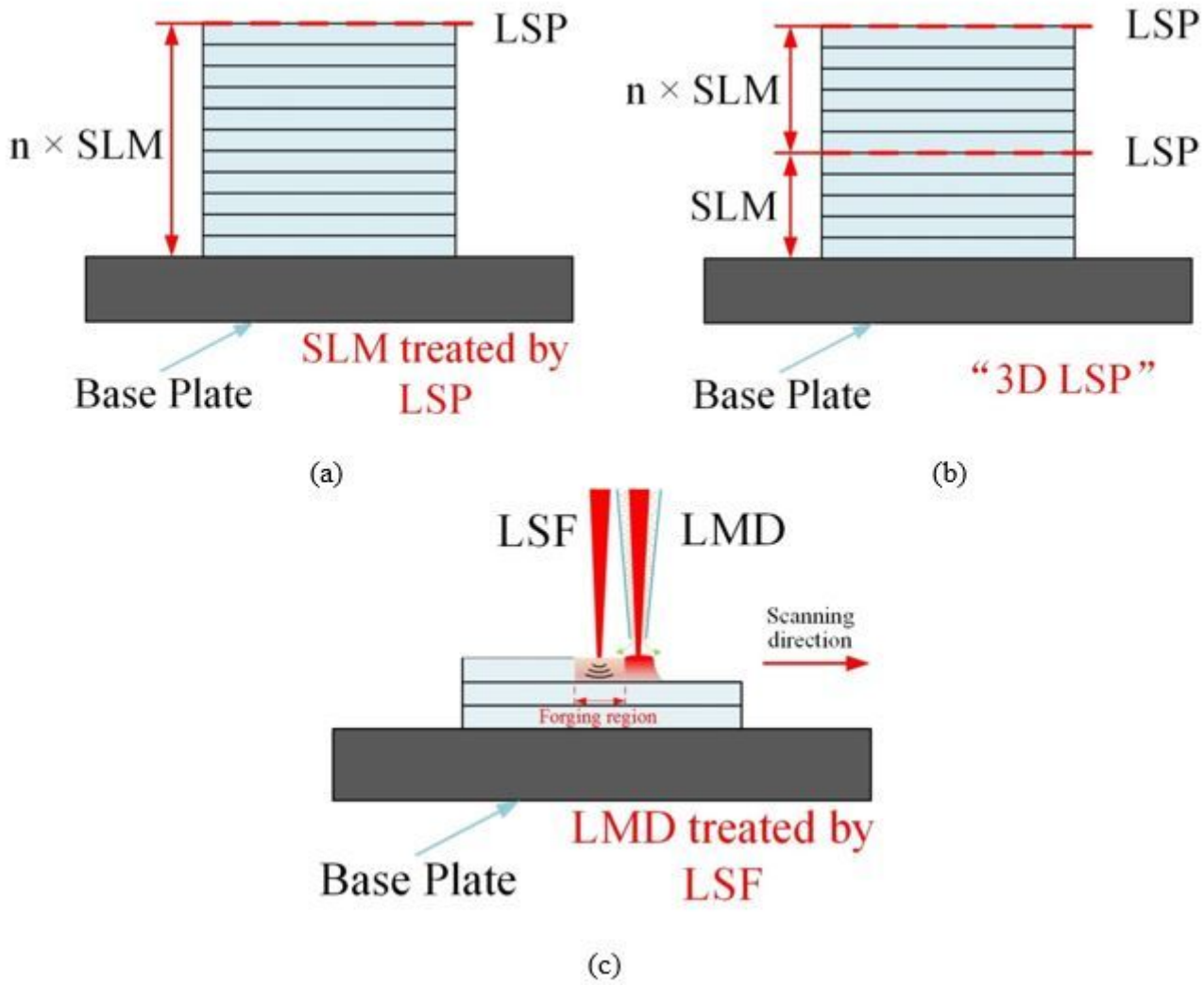

Figure 3

A schematic view of laser shock forging and comparison with LSP and "3D LSP". (a) SLM parts treated by LSP (b) "3D LSP" (c) LMD built parts treated by LSF

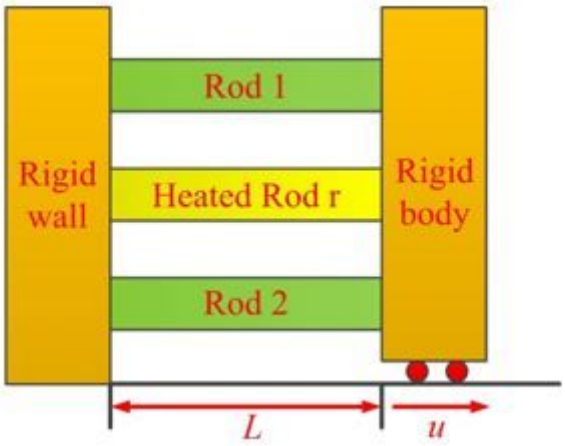

Figure 4

The classical Bar-frame model.

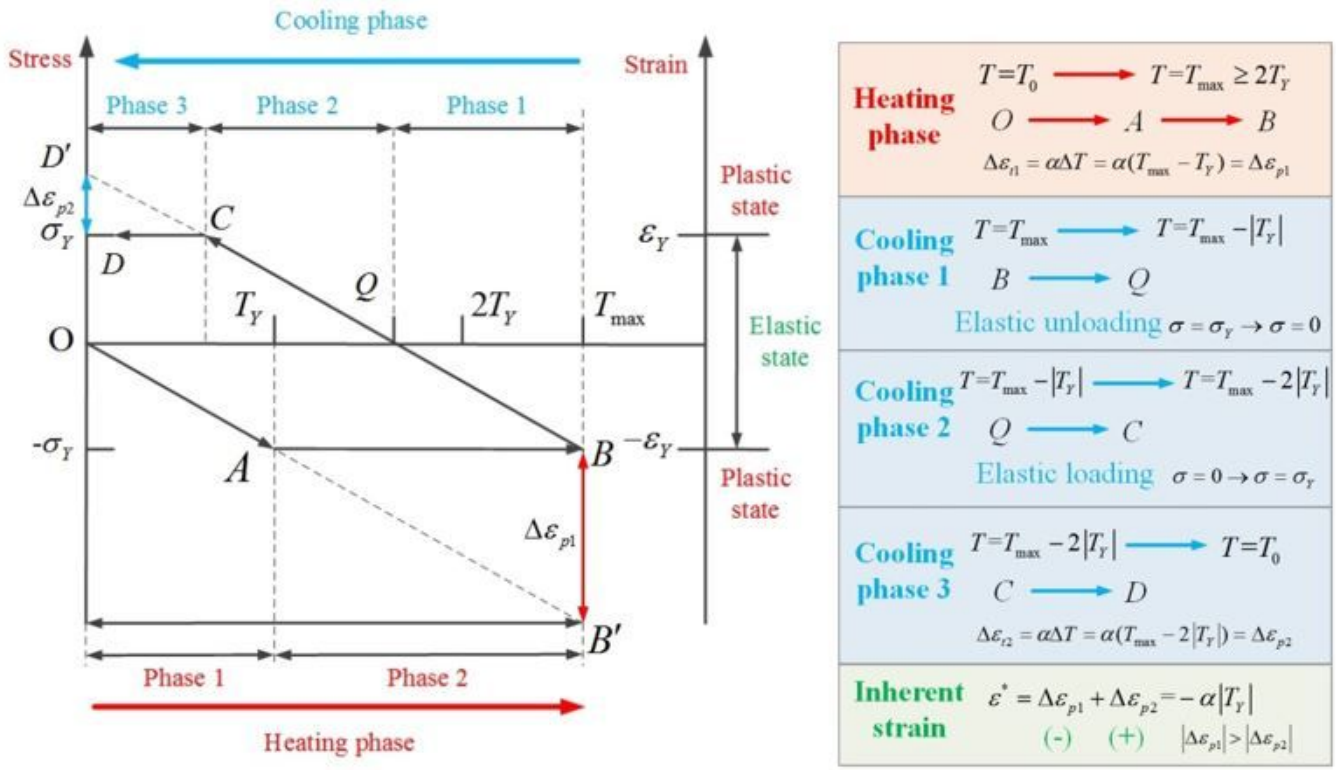

Figure 5

Stress and strain evolution at different heating and cooling stages.

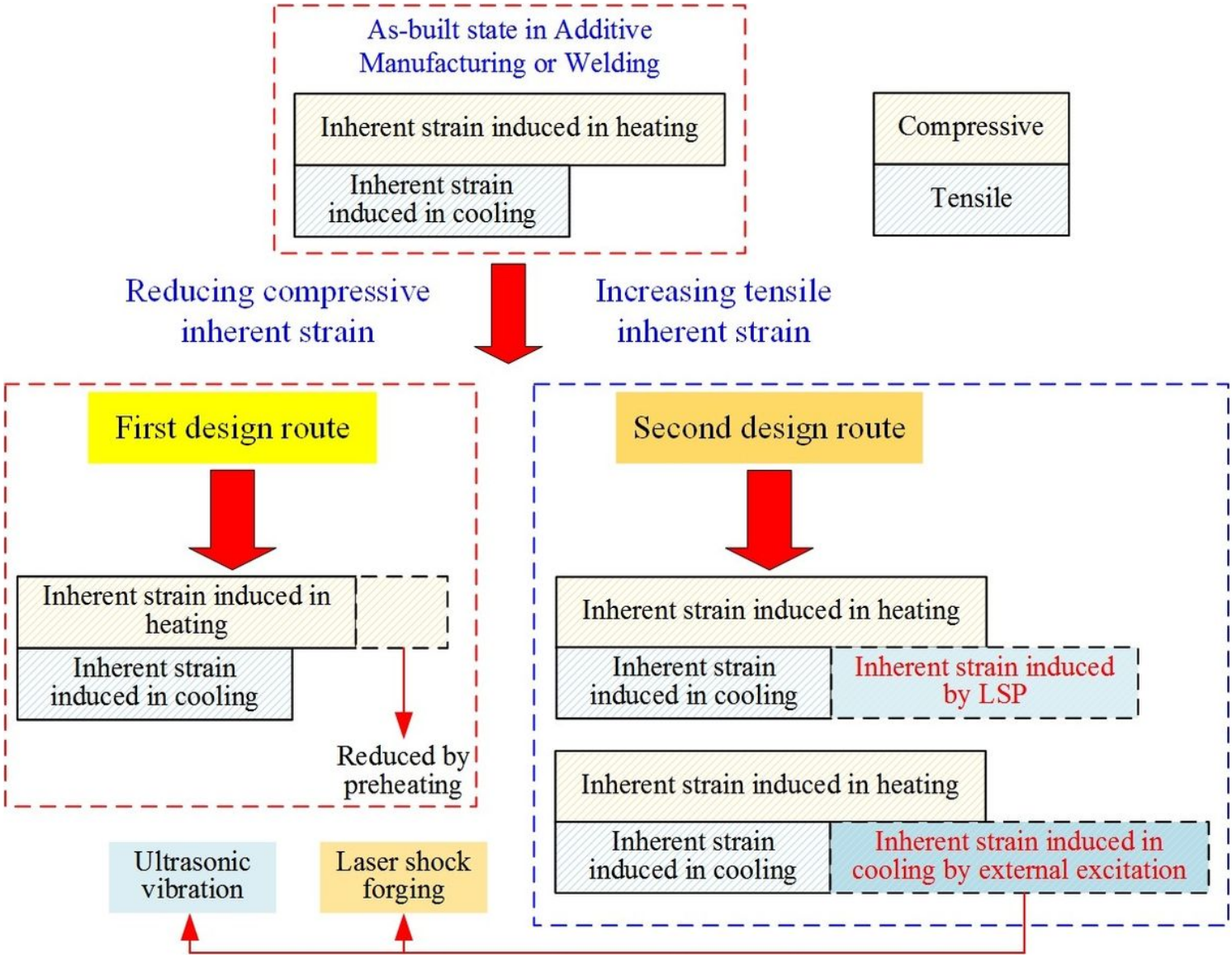

Figure 6

Two routes towards reducing inherent strain in additive manufacturing or welding

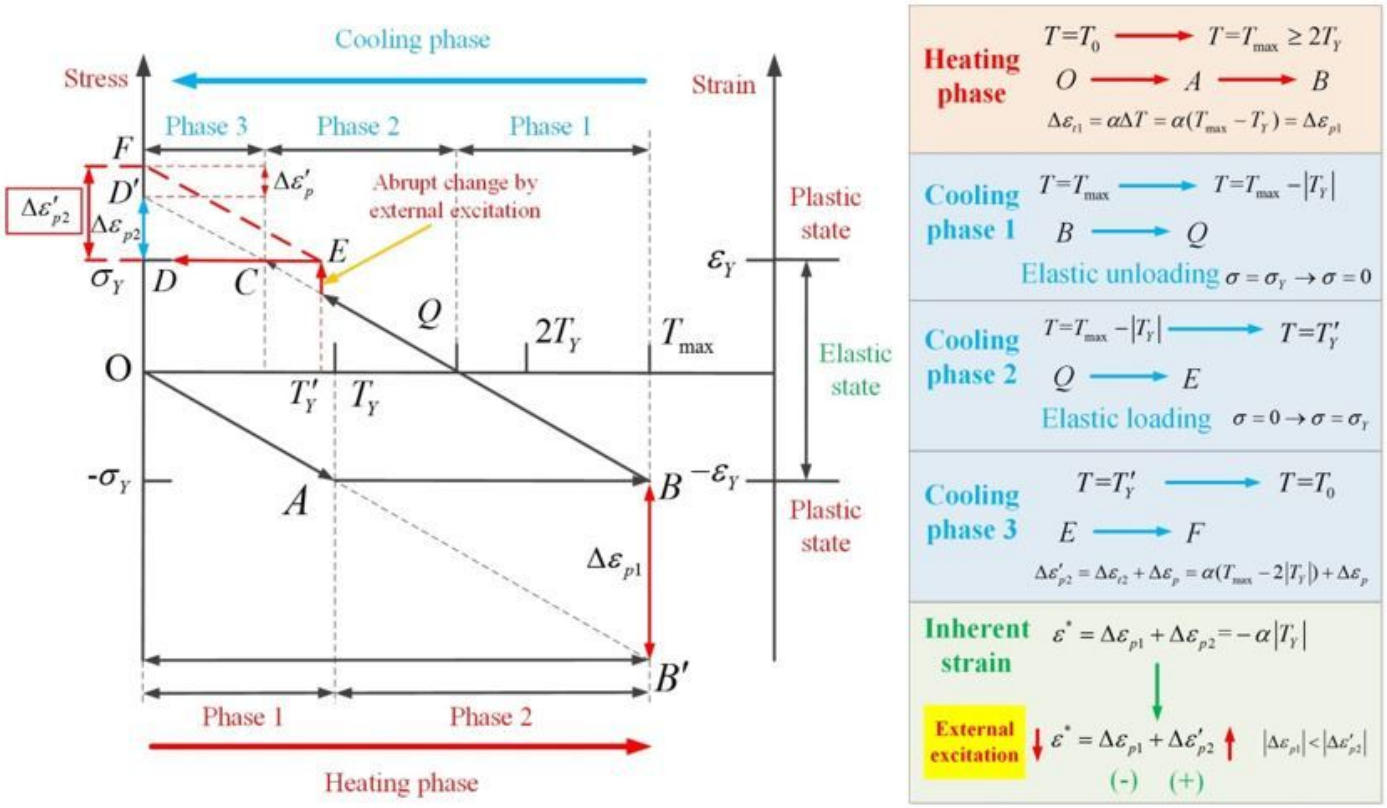

Figure 7

Stress and strain evolution at different heating and cooling stages if external excitation is imposed

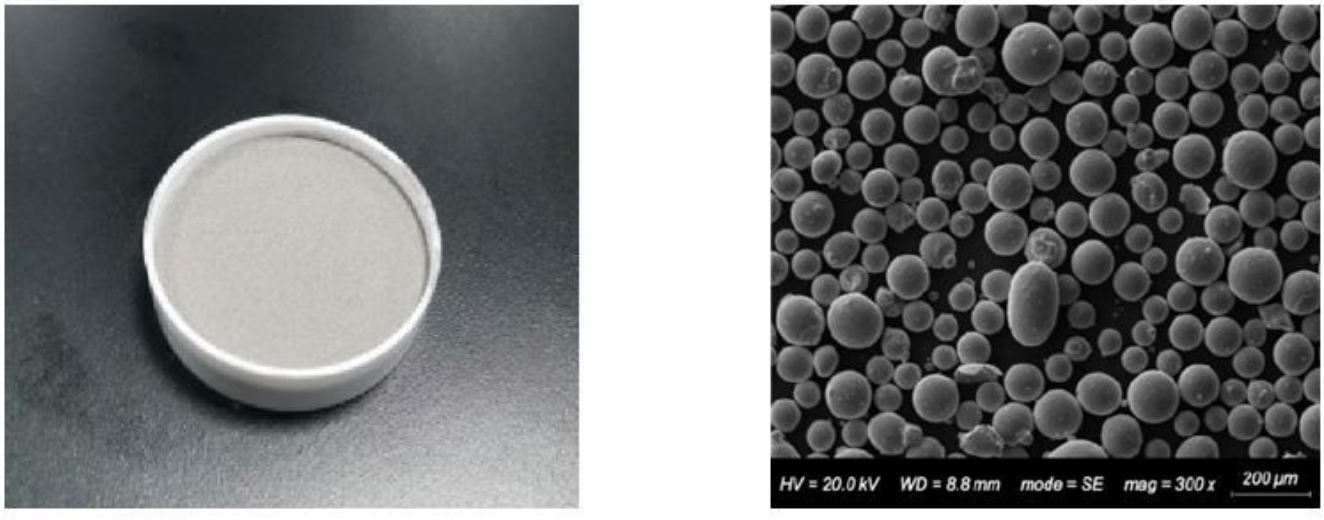

(a) (b)

Figure 8

Macro and micro morphology of 316L stainless steel powder. (a) Marco (b) Micro

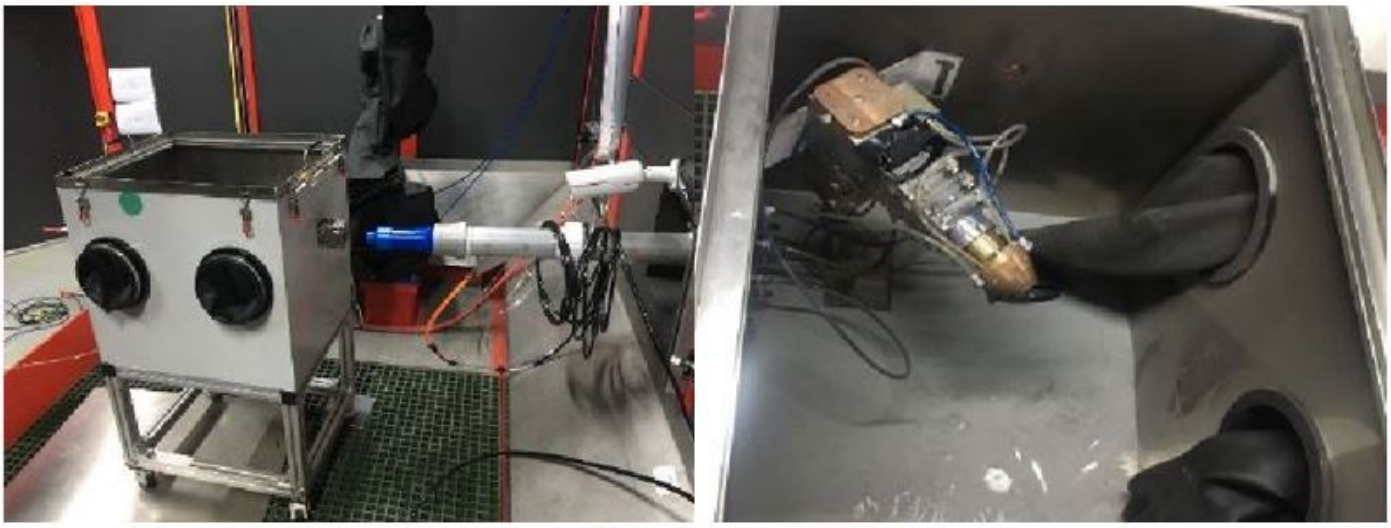

Figure 9

Laser metal deposition device. (a) External view (b) Internal view

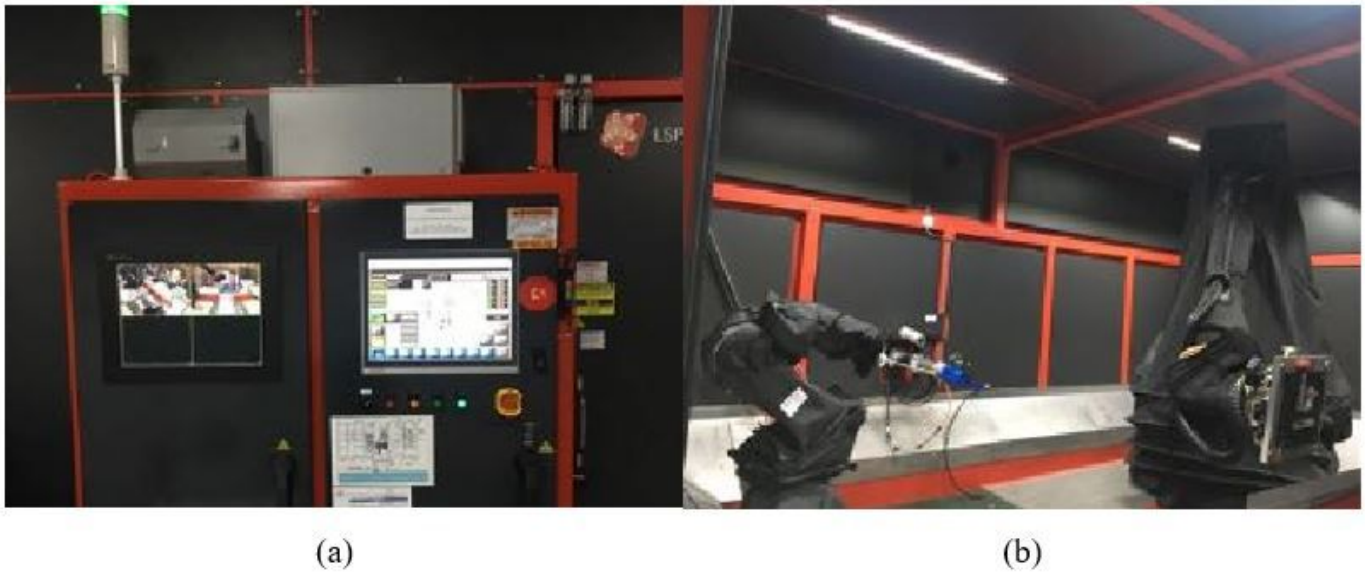

Figure 10

Laser shock peening device. (a) Control unit (b) Laser shock peening unit

Figure 11

XL-640X X-ray stress tester

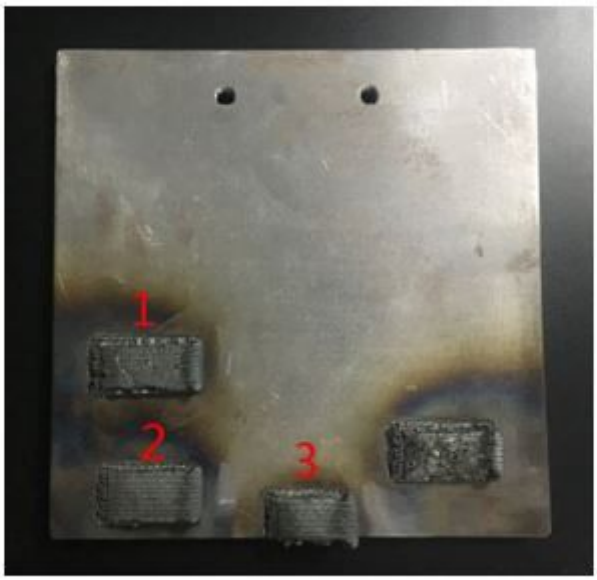

Figure 12

As-built specimens by LMD.

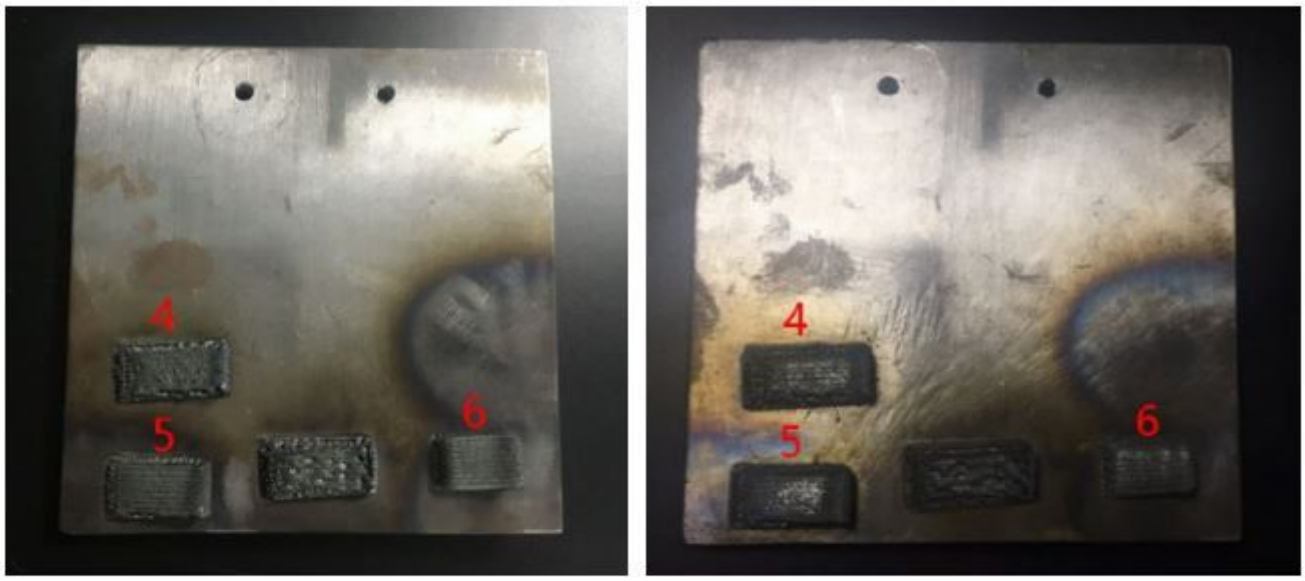

Figure 13

Specimens built by LMD before and after LSP. (a) Before (b) After

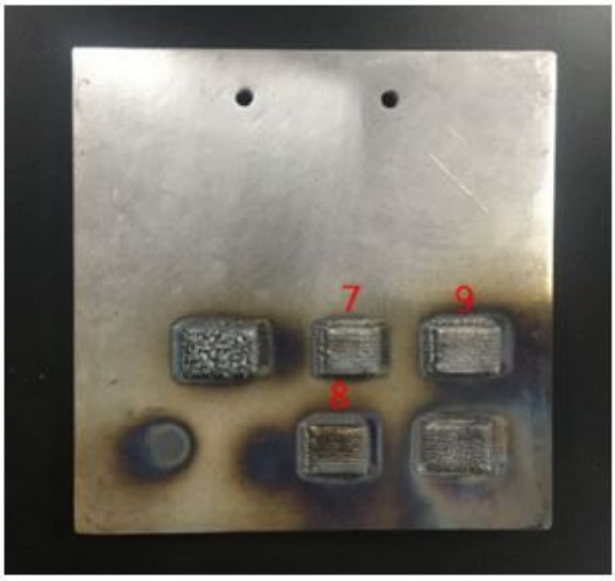

Figure 14

Specimens built by LMD combined with LSF.

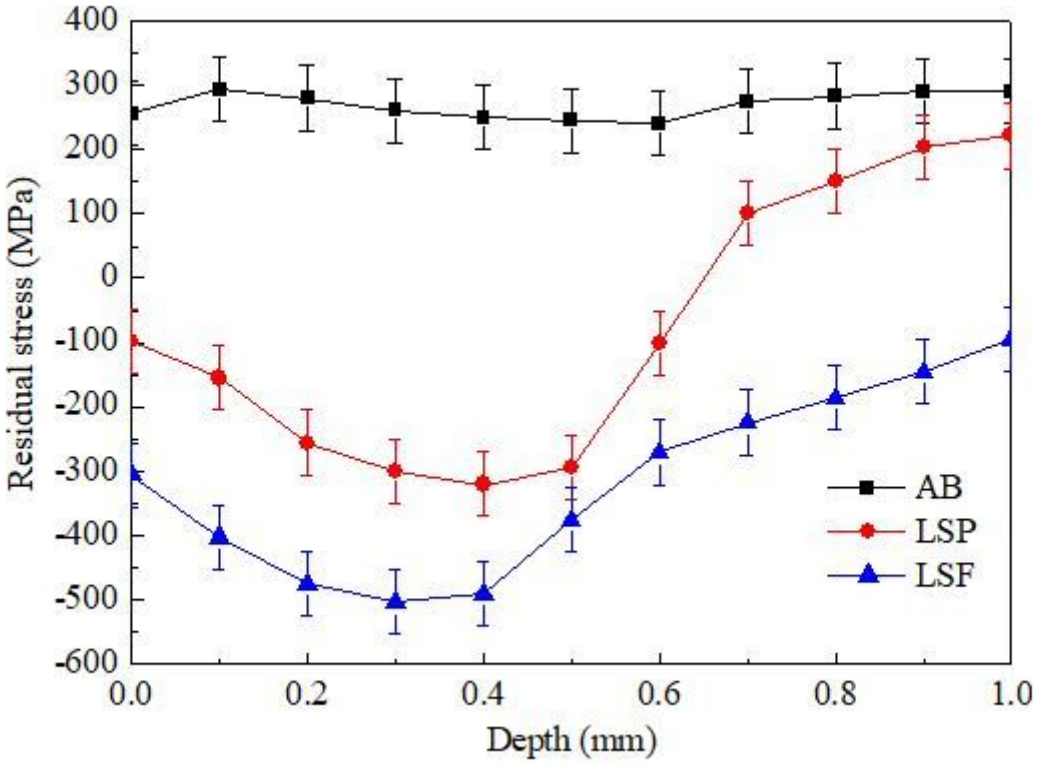

Figure 15

Residual stress profiles measured for specimens treated by different techniques.